ELSEVIER

Journal of Structural Geology 28 (2006) 902–918

JOURNAL OF STRUCTURAL GEOLOGY

www.elsevier.com/locate/jsg

Quartz veins deformed by diffusion creep-accommodated grain boundary sliding during a transient, high strain-rate event in the Southern Alps, New Zealand

Ruth H. Wightman [a,*], David J. Prior [b], Timothy A. Little [a]

[a] *School of Earth Sciences, Victoria University of Wellington, P.O. Box 600, Wellington, New Zealand*
[b] *Department of Earth and Ocean Sciences, Liverpool University, Liverpool L69 3GP, UK*

Received 1 October 2004; received in revised form 26 January 2006; accepted 14 February 2006
Available online 18 April 2006

Abstract

The crystallographic preferred orientations (CPOs) and microstructures of deformed quartz veins were measured for four samples in the hanging-wall of the Alpine Fault in the Southern Alps, New Zealand. Their deformation and exhumation has occurred since 4 Ma. The quartz veins have been ductilely sheared to finite shear-strains of 5–15 in late Cenozoic shear zones at 450 ± 50 °C, 310 ± 90 MPa and strain-rates between 2×10^{-11} and 2×10^{-9} s^{-1}. The sheared veins have a polygonal microstructure with few subgrains and an average grain-size of ~100 μm. The CPO of the veins is random to very weak within the shear zones. We suggest that dislocation creep accommodated initial shear deformation, at high stresses and strain-rates. The deformation must have created a strong CPO and concomitant dynamic recrystallization reduced the grain-size significantly. Dissipation of stresses during initial deformation lead to a stress and strain-rate drop required for a switch to diffusion creep-accommodated grain boundary sliding (GBS). Continued shearing accommodated by GBS destroyed the CPO. Post-deformational grain growth gave rise to a final polygonal microstructure with a similar grain size in veins and in the wall rocks. Analysis of existing experimental data suggest that this sequence of events is possible in the time available. Rates of all processes may have been enhanced by the presence of a water-rich fluid within the shear zones. These observations of naturally deformed rocks provide a model for the processes that may occur during short-lived deformation at transiently-high stresses at mid-crustal depths or deeper.

Keywords: Neotectonics; Quartz deformation; Southern Alps; Grain boundary sliding

1. Introduction

Structural geologists have long tried to relate microstructures and crystallographic fabrics to their causative deformation mechanisms, in both natural and experimental studies (e.g. Schmid, 1982; Hirth and Tullis, 1992). Crystallographic preferred orientations (CPOs) can be used to constrain deformation processes, with the presence of a CPO in rocks deformed in the solid-state indicating a deformation mechanism that is controlled by crystallography, i.e. dislocation creep or twinning (see reviews in Lister, 1977; Wenk and Christie, 1991; Gleason et al., 1993). The absence of a CPO in deformed rocks is often taken as evidence that the dominant deformation mechanism did not involve dislocation creep or other types of intracrystalline plasticity, but was instead controlled by diffusion or frictional-accommodated grain boundary sliding (GBS) (Law, 1990; Prior et al., 1999). CPOs record the last deformation event prior to microstructural freezing-in as the rocks were cooled and unroofed; in shear zones, CPOs in sheared quartzose rocks are typically reorganised at shear-strains as low as 2–3 (Brunel, 1980), although microstructural stability may not achieved until shear strains of ~5 (e.g. Pieri et al., 2001).

Our knowledge of CPOs and deformation mechanisms has been greatly enhanced through experimental data (e.g. Tullis, 1977; Wenk, 1985; Dell'Angelo and Tullis, 1989) and microtextural studies using optical microscopy combined with an array of specialised techniques, including electron channelling patterns (e.g. Lloyd, 1987; Lloyd et al., 1997) and X-ray texture goniometry (e.g. Schmid et al., 1981; Law, 1990). Quantitative microstructural, CPO and misorientation data can now be collected faster and more easily with electron back-scattered diffraction (EBSD) on the scanning electron

* Corresponding author.
E-mail addresses: ruth.wightman@vuw.ac.nz (R.H. Wightman), davep@liverpool.ac.uk (D.J. Prior), timothy.little@vuw.ac.nz (T.A. Little).

0191-8141/$ - see front matter © 2006 Elsevier Ltd. All rights reserved.
doi:10.1016/j.jsg.2006.02.008

microscope (SEM) (e.g. Trimby et al., 1998; Fliervoet et al., 1999; Prior et al., 1999; Jiang et al., 2000; Orzol et al., 2003; Barnhoorn et al., 2004; Bestmann et al., 2004; Borghi and Spiess, 2004), allowing detailed investigation into the microstructural signatures produced by different deformation mechanisms.

Deformation of quartz by mechanisms including dislocation creep and diffusion creep-accommodated GBS has been achieved in laboratories at experimental strain-rates of 10^{-5}–10^{-7} s^{-1} and temperatures >1000 °C (e.g. Hirth and Tullis, 1992; Brodie and Rutter, 2000). However, controversy exists as to whether diffusion creep and GBS can be the dominant deformation mechanism in quartz-rich rocks under natural conditions of temperature and strain-rate, due to the uncertainty in extrapolation of these experimental data. Under geological conditions, very fine grain-sizes (1–2 μm) and/or high fluid content are apparently necessary to allow GBS to occur, with many believing that very high temperatures (>700 °C) are a further prerequisite (e.g. Brodie and Rutter, 2000), such that GBS in quartz rarely occurs in nature. Furthermore, identifying GBS-accommodated deformation in natural examples is problematic, particularly if this is accompanied by or post-dated by dislocation creep-accommodated deformation. For these reasons, the presence or absence of GBS as an important deformation mechanism in naturally deformed samples remains a controversial topic (e.g. Behrmann and Mainprice, 1987; Fliervoet and White, 1995).

We present CPO and microstructural data from EBSD analyses of four quartz veins deformed to shear-strains of 5–15 in ductile shear zones in the hanging-wall of the Alpine Fault in the Southern Alps, New Zealand. These neotectonic shear zones provide a valuable opportunity to study recently quenched quartz microstructures in a geodynamically well-constrained natural laboratory.

2. Geologic and tectonic context of the samples

The samples used in this microstructural analysis are from quartz veins deformed by late Cenozoic ductile shear zones in the central Southern Alps, New Zealand (Fig. 1). The Southern Alps occur in the oblique collision zone between the Pacific and Australian plates, a result of rapid uplift that is focussed

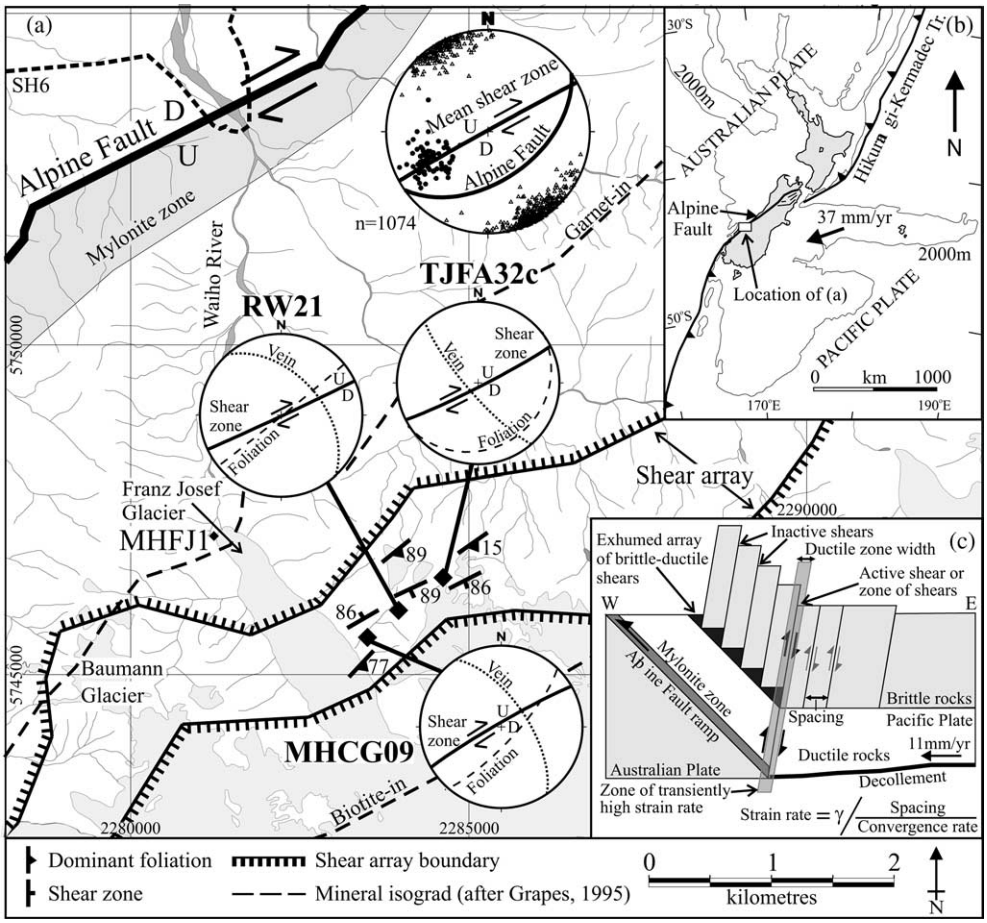

Fig. 1. Geodynamic context of EBSD samples: (a) simplified geologic map of the Franz Josef Glacier region, showing sample structural data and boundaries of the brittle-ductile shear array. Large stereonet is a synoptic of the brittle-ductile shear array, with slip lineations (filled circles) and poles to shear zones (open triangles) shown. EBSD sample locations (black diamonds) have stereographic representation of structural data. Trace of Alpine Fault from Norris et al. (1990). Graticules in New Zealand Map Grid coordinates (m). (b) Tectonic setting of New Zealand, showing major tectonic features and the location of (a). Plate motion vector from Walcott (1998). (c) Schematic diagram through Southern Alps orogen showing backshear-like nature of the brittle-ductile shear array and relationship to uplift on Alpine Fault ramp at depth after Little et al. (2002). Note dipping locus of high shear strain-rate in region of shear formation. No erosion is shown.

along the oblique-reverse Alpine Fault (Fig. 1b). In the central Southern Alps, the current plate motion vector trends ~071°, at a velocity of 39 mm yr^{-1} (De Mets et al., 1994). In the central Southern Alps, contemporary uplift of the fault's hanging-wall takes place at 5–10 mm yr^{-1} (Wellman, 1979; Bull and Cooper, 1986). Erosion-rates in the central Southern Alps are of comparable magnitude, preventing significant overthrusting of the Pacific Plate onto the Australian Plate and resulting in rapid exhumation of mid to lower crustal Pacific Plate rocks during the last 5 Ma (Koons, 1989; Little et al., 2005).

Despite the ~90 km of shortening across the Southern Alps since the inception of the Alpine Fault (Walcott, 1998), Pacific Plate rocks deeper than amphibolite grade rocks are not exposed at the surface. This suggests the presence of a mid-crustal décollement in the Pacific Plate at a depth of ~25–30 km (Wellman, 1979; Grapes, 1995). The hanging-wall of the Alpine Fault consists of the Alpine Schist, a Mesozoic sequence that has been tilted to the east during its uplift along the Alpine Fault (Fig. 1c). These quartzofeldspathic schists range in grade from prehnite-pumpellyite facies at the Main Divide to the east, through to garnet-oligoclase zone in the amphibolite facies rocks against the Alpine Fault to the west (Grapes, 1995). The main phase of metamorphism of these rocks is unrelated to the late-Cenozoic phase of convergence and uplift along the Alpine Fault (Norris et al., 1990; Grapes, 1995) and is late Cretaceous in age (Vry et al., 2004). Subsequent to this Barrovian metamorphism, further deformation, mineral growth and recrystallization took place in the late Cenozoic before and during unroofing of the rocks on the Alpine Fault (Little et al., 2002). The dominant foliation in the rocks, referred to as the Alpine foliation, lies slightly oblique to the strike of the Alpine Fault (Fig. 1a). In the late Cenozoic this fabric was strongly reinforced but also crosscut by dextral-oblique shear zones that strike parallel to the Alpine Fault (Fig. 1; Little et al., 2002).

3. Brittle-ductile shear zones in the Alpine Fault hanging-wall

The narrow ductile shear zones that deform the quartz veins examined in this study are located in biotite zone rocks of the Alpine Schist, ~7 km structurally above the southeast dipping Alpine Fault (Figs. 1, 2 and 3a). Accommodating deformation of the Alpine Fault's hanging-wall, these planar shear zones are near vertical and together comprise a 1.5-km-thick array that strikes and dips subparallel to the underlying Alpine Fault. The shears are the youngest ductile fabric in the Alpine Schist, cross-cutting all other fabric elements (Figs. 2a and 3b and c). They strike subparallel to the Alpine fault and are remarkably systematic in their spacing (mean 0.6±0.4 m), dextral-oblique kinematics (NW-up throw) and slip magnitude (mean 15.2±1.4 cm; Figs. 2a and 3b and c). Pre-deformational quartz veins are ductilely or brittle-ductilely sheared whereas the quartzofeldspathic host rock to the veins is generally brittlely faulted by the same shears (Figs. 2a and 3b and c). Offsets of the deformed veins over ductile zone widths of ~1.5±0.4 cm

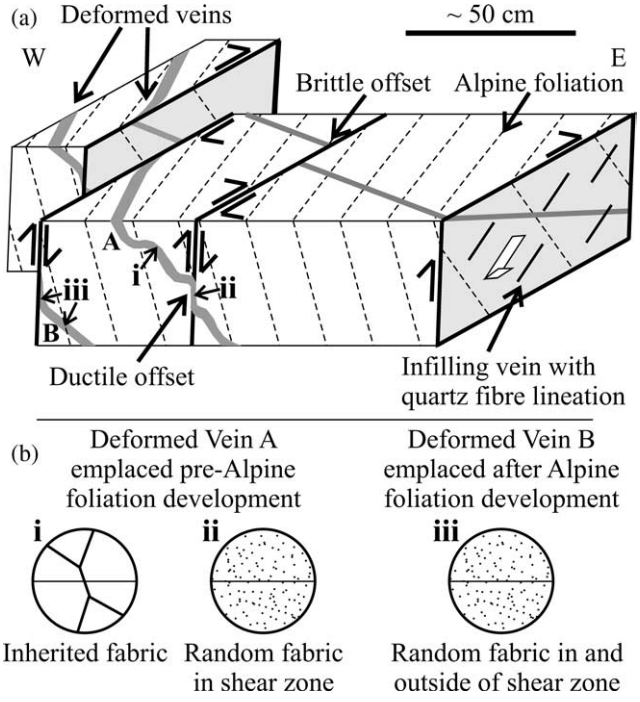

Fig. 2. (a) Schematic diagram showing detailed geometry of shear related deformation, both brittle and ductile offsets of veins and slip lineation along shear zone surface. (b) Schematic CPO fabrics in veins of different ages shown in (a). Vein A is emplaced prior to Alpine foliation development and has an inherited fabric (i) that corresponds to this deformation. Within the shear zone, Vein A's fabric is randomised (ii) by the proposed deformation model (see text for details). Vein B is emplaced after the development of the dominant Alpine foliation, and therefore has a random CPO both within and external to the shear zone (iii).

indicate finite ductile shear-strains of 10.1±2.8 per shear (n=1000). In addition, the shear zones are infilled with syntectonic quartz-calcite veins that range in thickness from 1 mm to several cm (Figs. 2a and 3b). These veins are evidence of fluid flow in the shears during their activity (Wightman et al., submitted).

We have interpreted the array as a sequence of back-shears related to the late-Cenozoic ramping and uplift of the Pacific Plate onto the moderately-dipping plane of the Alpine Fault (e.g. Little et al., 2002). The shears were apparently activated in a sequential escalator-like fashion to accommodate tilting of the delaminated Pacific Plate rocks onto the SE-dipping Alpine Fault ramp at depth (Fig. 1c). Such a back-shearing process has been simulated in numerical modelling of convergent deformation in two-sided orogens (e.g. Braun and Beaumont, 1995). Importantly here, these models show rocks in the vicinity of the lower ramp-step being subjected to transiently high stresses and strain-rate as they are jacked up onto the fault ramp at depth (Fig. 1c).

3.1. Deformation conditions

The escalator model of shear formation allowed an estimate of strain-rate for these structures to be derived from the known plate convergence-rate and spacing of the shears. Assuming sequential activation of the shears in an escalator-like fashion,

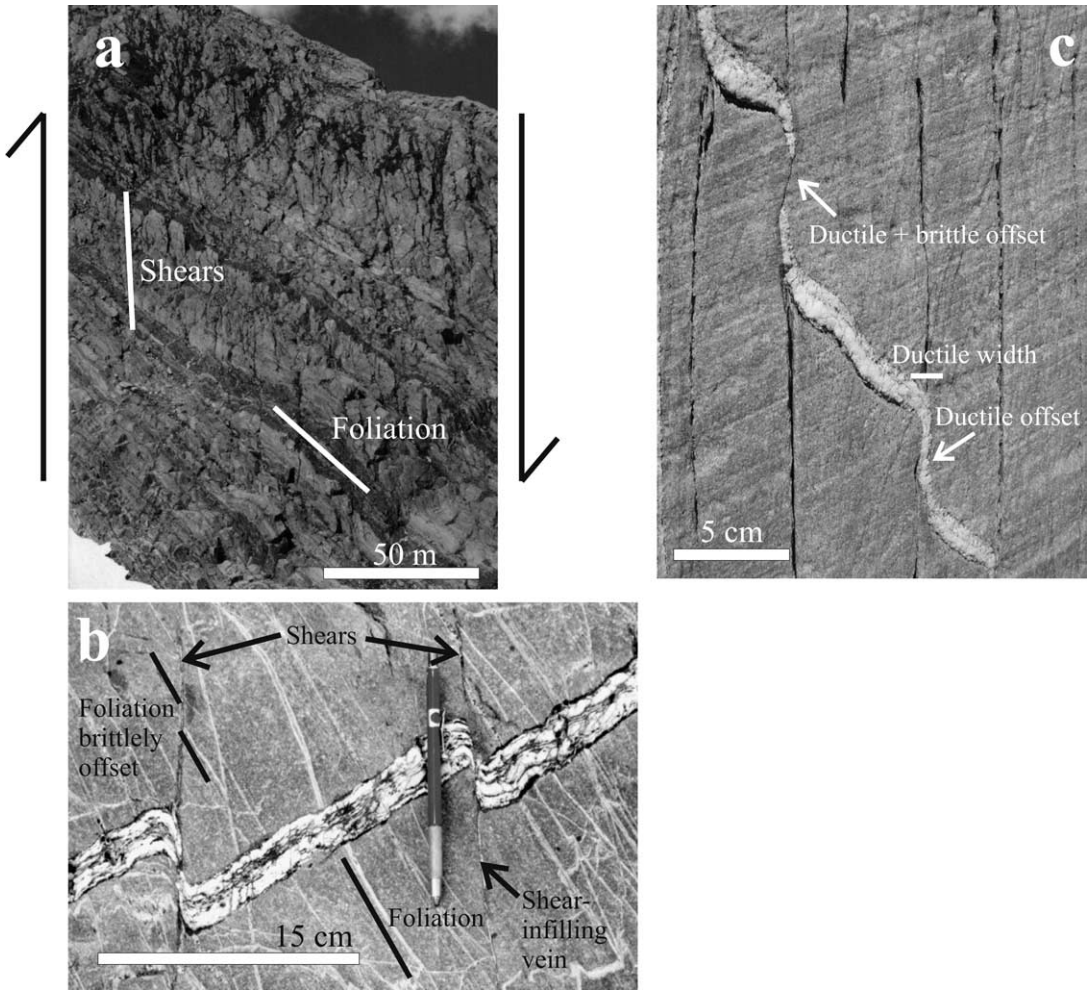

Fig. 3. Photographs (looking NE, parallel to strike of Alpine Fault) of late Cenozoic brittle-ductile shears exposed on the east side of the Franz Josef Glacier. Note the systematic spacing, consistent sense of throw and offset along the shears with respect to the main foliation and older quartz veins. (a) Shears exposed on a vertical cliff face. (b) Vein showing both brittle and ductile offsets. Note quartz-calcite vein infilling shear zone. (c) 1-cm-thick quartz vein offset through multiple shear zones.

a time estimate on the lifetime of an individual shear was made by dividing the average shear spacing by the plate convergence velocity normal to the Alpine Fault (11 ± 1.5 mm yr^{-1}; Walcott, 1998). Combined with the average ductile shear strain per shear, this analysis yields a mean strain-rate of $1.8 \times 10^{-9} \pm 5 \times 10^{-10}$ s^{-1} but is here assumed to overestimate the true rate because of the limiting assumption that only one shear is active at a time (Fig. 1c). In reality, multiple shears may have been active simultaneously across a zone of some finite width, thus extending the duration of shear activity beyond the minimum. For an active deformation zone width as wide as 100 m, the strain-rate would be reduced to 1.1×10^{-11} s^{-1}, which we will use as a minimum estimate of strain-rate.

Our estimated temperature of quartz deformation in the shear zones is 450 °C, which is consistent with several independent constraints. The shear zones are hosted by biotite zone, greenschist facies Alpine Schist that shows no low-temperature retrogression related to the shear deformation and fluid infiltration, implying deformation temperatures of ca. 350–550 °C. Estimates of the conditions of late Cenozoic metamorphism at structurally greater depths close to the Alpine Fault are lower amphibolite facies with deformation occurring up to ca. 600 °C (Vry et al., 2004), providing a maximum temperature for vein deformation. The shear-infilling veins themselves contain minor amounts of coexisting biotite and muscovite phases, which are stable together above ~380 °C, as well as coexisting clinozoisite ($\alpha_{czo} = 0.47$), quartz and calcite. The deposition temperature of these veins must lie on the low temperature side of the equilibrium reaction $2czo + 3qtz + 5cal = 3gr + 5CO_2 + H_2O$, giving a maximum temperature constraint of 500 °C. Together, these constraints place the temperature of shear zone deformation at 400–500 °C. Our preferred temperature was determined from oxygen isotope thermometry on quartz and calcite from the veins infilling the shear zones, estimating the temperatures of shear zone deformation as 450 ± 50 °C (Wightman et al., submitted) and this temperature will be used throughout this paper. However, it is important to bear in mind that the conclusions and model for shear zone deformation presented in this paper are independent of precise temperature and would be no less valid if a broader range of temperatures were invoked.

The geodynamic model to explain the shearing (Fig. 1c) suggests that the shears developed ~7 km higher in the crust

Table 1
Sample description and mineralogy

Sample	Original thickness of vein (cm)	Appearance of veins outside of shear zone	Minimum sheared thickness (cm)	Brittle offset (cm)	Ductile offset (cm)	Ductile width (cm)	Shear strain	Mineralogy[a]
TJFA32c	1.8	Planar	0.6	0	10.5	1.3	8	qtz, cal, *hem, rut*
RW21a	2.0	Folded[b]	0.7	2	8	0.8	13	qtz, cal
MHCG09	2.8	Planar	1.4	10	8	1.4	6	qtz, cal, *bt, chl, hem*

[a] Abbreviations after Kretz (1983); minerals in italics are present in trace amounts only.
[b] Vein folded about the dominant Alpine foliation.

than the basal décollement in the hanging wall, i.e. at depths of 18–23 km, with corresponding lithostatic pressures of ~490–620 MPa. Primary fluid inclusion analyses from the infilling veins, when combined with the estimated deformation temperature of 450±50 °C, indicate fluid pressures at the time of fluid inclusion trapping of 310±90 MPa (Wightman et al., submitted). These fluid inclusions were trapped subsequent to failure of the shear zones and therefore record a post-failure fluid pressure. Fluid pressures prior to shear zone failure were likely to have been higher, potentially as high as lithostatic pressure (Wightman et al., submitted).

4. Description of deformed quartz vein samples

The four samples analysed in this study are >1-cm-thick quartz±calcite veins that have been strongly and coherently deformed across the narrow, late Cenozoic shear zones, located in the Franz Josef Glacier region of the Southern Alps (Fig. 1a). Details of vein thicknesses, mineralogy, and amount of offset along the shear zones are presented in Table 1. Sample TJFA32c (p1 and p2, Fig. 4) embraces a complete profile across a 1.8-cm-thick deformed quartz-calcite vein that is smoothly and continuously deflected from one side of the shear zone to the other. RW21a and MHCG09 are 2.0- and 2.8-cm-wide quartz-calcite veins, respectively, that have been displaced across shear zones with both brittle and ductile components of deformation (Table 1), perhaps reflecting changes in strain-rate during their deformation history. Although all the veins studied clearly predate the late Cenozoic shearing event, their original emplacement ages are unknown and may differ between the samples. Samples TJFA32c (p1 and p2) and MHCG09 are planar features outside of the shear zones (Fig. 4), cross-cutting the Alpine foliation, whereas sample RW21a is folded across the pre-existing fabric. Thus their inherited, pre-Cenozoic deformation history may be non-uniform. Both sheared and unsheared areas of these veins were analysed.

5. Analytical procedures

5.1. Imaging techniques

Thin sections, 30 μm thick, were made from the deformed veins, cut perpendicular to the shear zone boundary and parallel to the quartz-chlorite fibre lineation on the shear zone surface (Fig. 4). Standard optical microscopy was used to assess the microstructure of each sample (Fig. 5) prior to mechanical and chemical (using Syton fluid) polishing in preparation for EBSD analyses (for details of preparation methodology, see Lloyd (1987) and Prior et al. (1999)). The thin sections were coated with a thin carbon coat in order to reduce charging effects during SEM work. Cathodaluminescence was carried out on a Philips XL 30 SEM using an accelerating voltage of 10 kV and a beam current of ~1 nA. EBSD analyses were undertaken using a CamScan X500 crystal probe fitted with a thermionic field emission gun and a FASTTRACK stage. The SEM was operated with an accelerating voltage of 20 kV and a beam current of 30 nA, and a working distance of 24 mm was used.

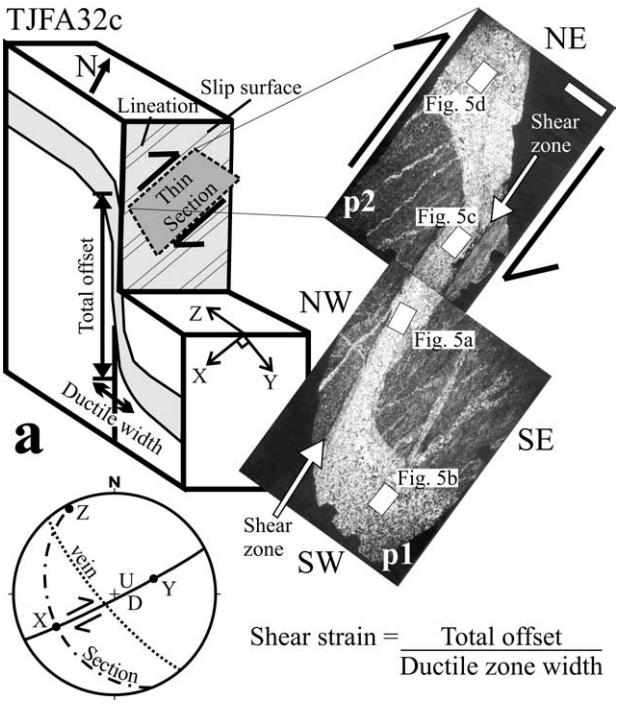

Fig. 4. Schematic diagram of sample outcrop, TJFA32c. Diagram is oriented upthrown to the northwest, showing magnitude of offset (does not show strike-slip offset component). Thin sections are cut perpendicular to the shear zone surface (shown in pale grey) and parallel to the slip lineation (shown stereographically). Photographs of whole thin sections (p1 and p2) are taken under cross-polarised light, incorporating part of the sheared vein and a section outside of the shear zone, with shear sense shown. Scale bar is 1 cm long. Note location of photomicrographs shown in Fig. 5.

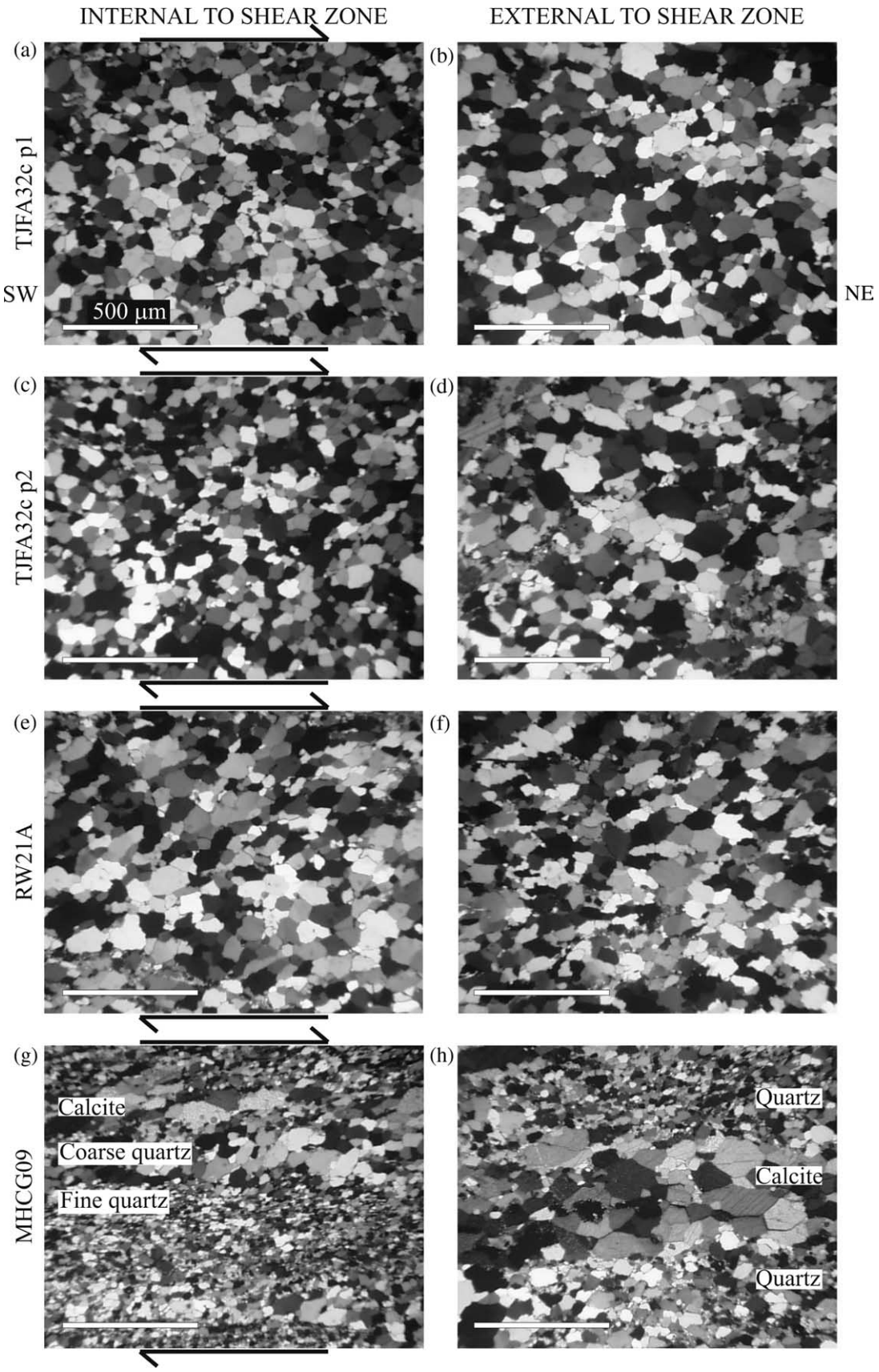

Fig. 5. Photomicrographs taken under cross-polarised light of sheared and unsheared sections of samples. Note the polygonal quartz microstructure and absence of undulose extinction or subgrains. Scale bar is 500 μm long. TJFA32c p1 from within (a) and outside (b) of the shear zone. TJFA32c p2 from within (c) and outside (d) of the shear zone. RW21a from within (e) and outside (f) of the shear zone. MHCG09 from within (g) and outside (h) of the shear zone.

Table 2
Summary of data collected and collection method during EBSD analyses

Sample	Vein type	Area sampled	Sampling strategy	Phases indexed	Mean grain size[a] (μm)	No. grains sampled
RW21a	Sheared	25×1 mm	10 μm step size; map	Qtz	90 (>400)	3414
	Unsheared	2.4×11 mm	10 μm step size; map	Qtz	90 (400)	3252
TJFA32c-p1	Sheared	5×1 mm	10 μm step size; map	Qtz	85 (>350)	711
	Sheared	2.3×7.7 mm	10 μm step size; map	Cal+qtz	cc 90 (>300)	1382 (cc)
	Unsheared	2×6 mm	10 μm step; 4×4 grid; 200 μm spacing	Qtz	NA[b]	297
TJFA32c-p2	Sheared	24×1 mm	10 μm step size; map	Qtz	80 (>400)	4511
	Unsheared	2.3×10 mm	10 μm step size; map	Qtz	75 (>580)	3078
MHCG09-p1	Sheared	6×5 mm	4 μm step size; map	Qtz+cal	qtz 50 (>250)	2277
	Unsheared	10×1.5 mm	10 μm step; 4×4 grid; 200 μm spacing	Qtz	NA[b]	366

[a] Maximum grain size given in parentheses.
[b] Unable to determine grain size due to sampling method.

5.2. Crystallographic techniques

EBSD patterns were collected on rectangular grids with a 10 μm spacing between data points in order to have multiple data points within each grain (working with an average quartz grain-size of 100 μm), although finer spacings and mapping strategies were occasionally used. Table 2 gives a summary of grid-size, spacing and area covered by each analysis. Two samples, the unsheared sections of TJFA32c p1 and MHCG09, were sampled on 4×4 grids of 10 μm step-size, with 200 μm spacing between each grid. This strategy allowed collection of crystallographic preferred orientations for each sample, without the time impediment of making an entire map, and the 4×4 grid allowed us to assess the reliability of the data in terms of indexing.

Each EBSD pattern was automatically indexed using the program *Channel5* from HKL software (only quartz was indexed in most samples, although analysis of the sheared section of MHCG09 indexed both quartz and calcite). Seven bands in the diffraction pattern were picked automatically, using the Hough transform routine built into the *Channel5* program. This enabled the absolute crystallographic orientation of each individual point analysed to be determined. The EBSD maps (Fig. 6) were made using a combination of beam and stage scans (for further

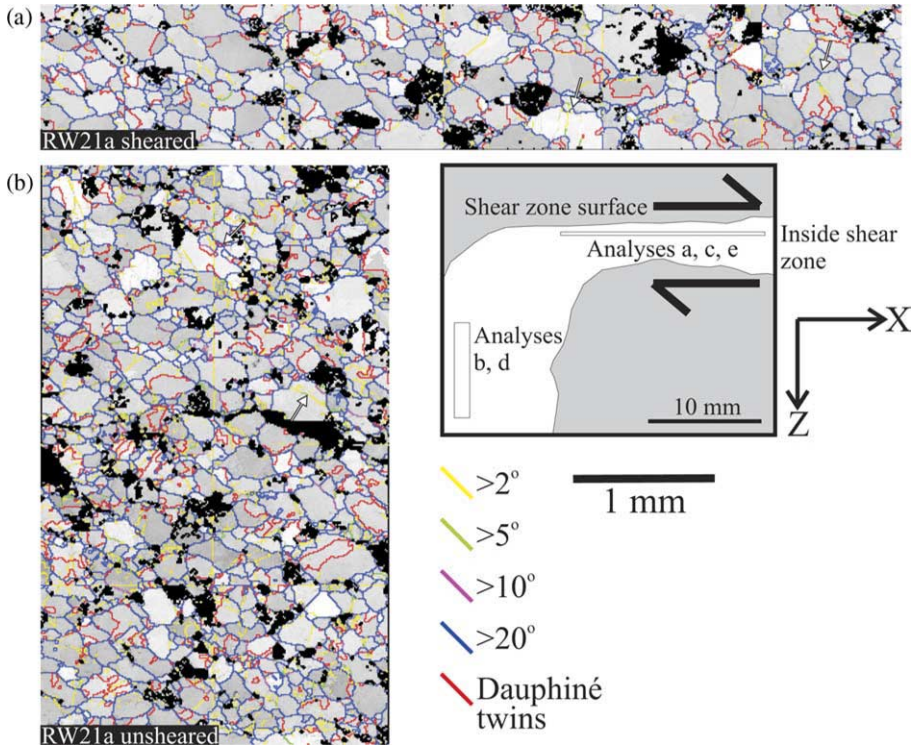

Fig. 6. EBSD pattern quality maps (very similar to orientation contrast images) showing misorientations between neighbouring pixels for sample RW21a. Subgrains are considered to have <10° misorientation (yellow and green boundaries). EBSD analyses only indexed a quartz phase. Points where no solution was obtained are shown in black. Step size 10 μm. Some linear misorientation features appear due to alignment along edges of stage scans. All images are extracted from larger processed maps (full maps are too large to reproduce here in any detail). (a) Sheared part of the vein. Arrows indicate straight and sutured grain boundaries. (b) Vein outside of the shear zone. Sutured grain boundaries and minor subgrains are indicated by the arrows.

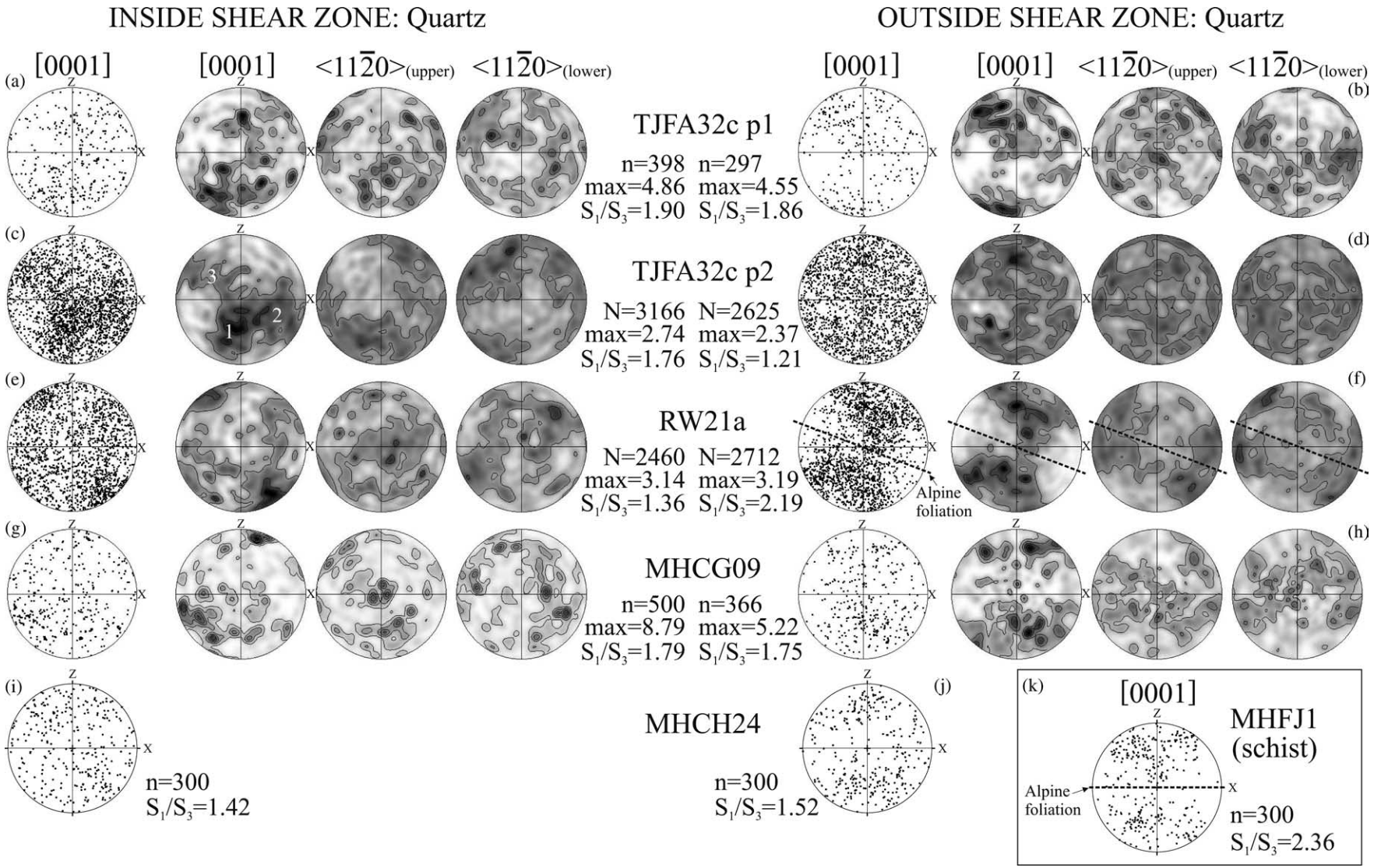

Fig. 7. Equal area lower hemisphere plots of c-axis and a-axes orientations. Plots are oriented SW–NE, where horizontal is parallel to the shear zone boundary, as shown in Fig. 4, except (k) where horizontal is parallel to the Alpine foliation. Contoured data is in multiples of uniform distribution. Max is the magnitude of the maxima for c-axis plots and S_1/S_3 is the ratio of the maximum and minimum eigenvalues. All plots use one point per grain (1ppg). TJFA32c p1 from within (a) and outside (b) of the shear zone. TJFA32c p2 from within (c) and outside (d) of the shear zone. RW21a from within (e) and outside (f) of the shear zone. MHCG09 from within (g) and outside (h) of the shear zone. (i)–(k) U-stage c-axes plots for samples MHCH24 inside and outside of the shear zone and schist sample MHFJ1, respectively, from Hill (2005).

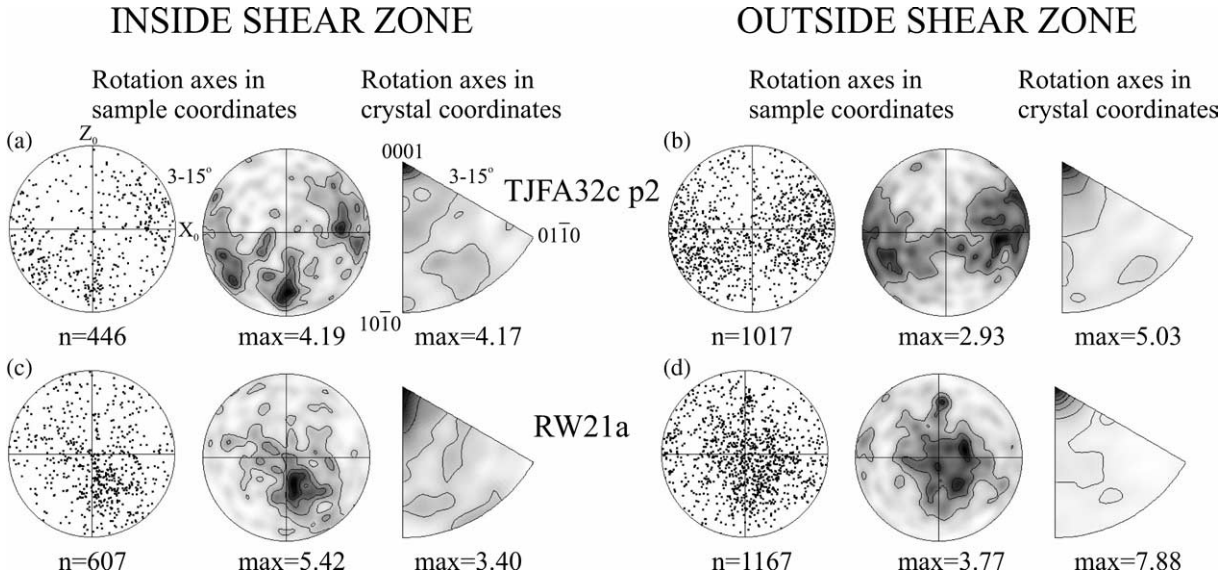

Fig. 8. Misorientation axes data for TJFA32c p2 ((a) and (b)) and RW21a ((c) and (d)) calculated from a subset of the orientation data, using only one point per boundary. This plotting technique eliminates the bias created by long boundaries when all misorientation data are plotted. Only rotation axes for misorientation angles between 3 and 15° are shown. Misorientation axes are displayed in the sample reference frame as equal area lower hemisphere plots and in the crystal reference frame as inverse pole figures. The orientation of sample reference axes with respect to the shear zone is shown in Fig. 6. Contoured data is in multiples of uniform distribution. Max is the magnitude of the maxima.

discussion of scan types and EBSD accuracy see Prior et al. (1999, 2002) and Bestmann and Prior (2003)).

5.3. Data analysis

Channel5 was used to process the data further, including the automatic removal of erroneous data or 'random spikes' (Bestmann and Prior, 2003). The program was also used to carefully 'grow' grains into grain boundaries, as these are in general regions that are poorly indexed by EBSD technique (Bestmann and Prior, 2003). Orientation maps (Fig. 6) were produced by plotting the calculated misorientations between neighbouring pixels onto pattern quality maps of the microstructure. These orientation maps are complementary to optical microscopy as part of a full microstructural description, as they quantify grain and subgrain boundaries. The maps for each sample analysed reveal very similar microstructures, as observed by optical microscopy (Fig. 5); therefore only orientation maps for sample RW21a are presented here (Fig. 6). The crystallographic orientations of the analysed grains were used to compile pole figures (Fig. 7). The minimum angular misorientation between neighbouring grains and their misorientation axes were calculated and plotted on inverse pole figures in the crystal and sample reference frames (Fig. 8; see Prior et al. (1999, 2002), Wheeler et al. (2001) and Fliervoet et al. (1999) for a detailed description of misorientation angle calculation).

6. Results of microstructural analyses

6.1. Microstructure

The four vein samples, TJFA32c p1 and p2, RW21a and MHCG09, consist of a granoblastic mosaic of quartz and calcite with remarkable similarities in appearance between the sheared and unsheared sections of the veins, although there are slight differences in grain size and the degree of annealing (Fig. 5). The parts of the veins external to the shear zones have a varied quartz grain-size, with an average size of ~100 μm but grains as large as 600 μm are present (Fig. 5; Table 2). Despite the range in grain-sizes in the veins outside of the shear zones, the quartz microstructure appears largely annealed, with minor sutured grain boundaries locally present and some evidence for intracrystalline strain in the form of minor subgrains and undulose extinction (Fig. 5).

Inside of the shear zones, quartz grain-sizes are slightly finer (average ~80 μm) than the adjacent unsheared part of the same veins, with fewer very coarse grains (Fig. 5; Table 2). Sample MHCG09 has a slightly bi-modal grain-size inside the sheared section of the vein, with coarse-grained (average 100 μm) bands of quartz approximately five grains thick, interlayered with finer grained (<50 μm) bands (Fig. 5g). In the central, strongly sheared part of all the vein samples, the quartz microstructure is remarkably polygonal, with common straight boundaries and 120° triple points. Although there is some localised, weak undulose extinction and some subgrains are present, most quartz grains in the sheared section of the veins appear remarkably free of intracrystalline strain (Fig. 5). The quartz contains Dauphiné twins (red boundaries in Fig. 6) that are not visible optically, which are as common in the sheared veins as in the unsheared sections, suggesting that the Dauphiné twins in these samples were not created during shear zone deformation. SEM-CL images of RW21a showed no substantial differences in CL intensity across the boundaries of the shear zone (see supplementary data). There are some discrete patches of brighter CL at the margins of a few isolated grains, which may represent infilling or overgrowth but there

are not enough of these features to identify any significant pattern.

The samples contain calcite (average grain size 90 μm; Table 2) that is generally restricted to bands, 2–3 grains wide, which are oriented subparallel to one another and to the vein margins in the areas outside of the shear zones (Fig. 5h), but which have been sheared into parallelism with the shear zone walls inside of the sheared section of the veins. These sheared calcite bands contain a strong grain-shape fabric, with the long axes of the grains oriented parallel to the shear zone margin (Fig. 5g). External to the shear zone, the calcite bands in sample RW21a are crenulated across the dominant Alpine foliation in the surrounding schist host rock. This suggests that RW21a preserves part of the pre-late Cenozoic deformation history and that the vein was emplaced prior to the development of the Mesozoic Alpine foliation.

6.2. Crystallographic preferred orientation (CPO)

Fig. 7 shows CPO data plotted as one point per grain, which has the advantage of removing the bias of any large grains that are represented by multiple measurements. Where the sampling strategy differed (see Table 2), each point represents one manually selected grain. Sections are oriented with respect to the shear zone boundary of the sample, with X parallel to the lineation and the boundary, as shown stereographically in Fig. 4.

TJFA32c shows a weak CPO outside of the shear zone in both samples (i.e. TJFA32c p1 and TJFA32c p2; Fig. 7b and d), as is consistent with the apparent lack of fabric or foliation in the unsheared vein (Fig. 2b). Inside the shear zone, the fabric in TJFA32c p1 (Fig. 7a) is not well defined, but may possibly represent a very weak single girdle of c-axes (although the eigenvalue ratio $S_1/S_3 = 1.90$, reflecting the clustering of points in one orientation; Fig. 7a), consistent with dextral-oblique shear. However, the sheared section of TJFA32c p2 (Fig. 7c), which is another part of the same vein as -p1, shows a weak cross-girdle fabric that is clustered into three areas. These three clusters do not show any obvious kinematic significance as they do not exhibit monoclinic symmetry with respect to the shear zone boundary.

Fig. 7f shows the quartz phase of RW21a in the unsheared part of the vein to have a strong ($S_1/S_3 = 2.19$) asymmetric type-1, or possibly type-2 cross-girdle (Lister, 1977). This agrees with the microstructural observation that the vein has been folded and shortened across the Alpine foliation (Fig. 2b). The girdle is not perfectly centred about Y, but is slightly askew, consistent with the slight obliquity of the Alpine foliation to the shear zone boundary in this sample (Fig. 1a). Inside the shear zone, however (Figs. 2b and 7e), the CPO of the same vein is weak ($S_1/S_3 = 1.36$) but does show a slight clustering of c-axes slightly askew of the z-direction. An EBSD analysis from the transition between the sheared and unsheared section of the sample yielded a gradual randomisation of the cross-girdle fabric with increasing proximity to the shear zone.

Outside of the shear zone, MHCG09 shows a weak CPO fabric (Fig. 7h), which is consistent with the microstructural observation that calcite bands in this sample are not aligned parallel to an external foliation and the lack of folding due to Alpine foliation development evident in the unsheared vein (Fig. 2b). Similarly, inside the shear zone, MHCG09 has a very weak CPO (Figs. 2b and 7g), the statistically significant S_1/S_3 ratio (1.79) reflecting the clustering of points close to the z-axis, rather than the development of a distinctive single girdle fabric.

Multiple additional deformed vein samples have been analysed using the universal-stage (Hill, 2005) and two of these c-axes fabrics are also displayed in Fig. 7. Sample MHCH24, located ~10 km SW of the other samples analysed (see Hill (2005) for location), is a 1.4-cm-thick quartz vein, deformed to a shear strain of 6.8 by a brittle-ductile shear zone. Outside of the shear zone, the vein's fabric consists of two small circles (Fig. 7j), whereas inside of the shear zone the c-axes define a random fabric (S_1/S_3 ratio is less than 1.44, implying a statistically random pattern; Fig. 7i). A CPO plot of quartz c-axes measured inside a chert-rich band of the Alpine Schist (sample MHFJ1; Fig. 1a) reveals a strong type-1 cross-girdle ($S_1/S_3 = 2.36$; Fig. 7k), confirming the presence of a strong foliation in the schist external to the brittle-ductile shear zones.

6.3. Misorientation axis distributions

Plotted in Fig. 8 are rotation axes for misorientation angles between 3 and 15° for quartz in the sheared and unsheared sections of samples TJFA32c p2 and RW21a. Misorientation axis distributions from outside of the shear zone could not be generated for TJFA32c p1 and MHCG09 due to the sampling strategy (Table 2). Low-angle (3–15°) boundaries only were plotted as their formation relates directly to a plastic deformation mechanism such as subgrain rotation recrystallization. Higher-angle grain boundaries have random misorientation axes (not shown here), except for the dominance of 60° rotations about [0001] related to Dauphiné twin boundaries.

Overall, the unsheared samples have twice the number of low-angle boundaries than their sheared counterparts, reflecting the higher number of subgrains in the unsheared section of the veins (Fig. 8). This is consistent with the overall internally strain-free appearance of quartz grains inside of the shear zones (Fig. 5). In the crystallographic reference frame, low-angle misorientation axes are dominated by a rotation about the c-axis in both the sheared and unsheared sections of the veins. This observation is indicative of slip on the prism planes, most likely prism-⟨a⟩ slip, considered to be a higher temperature (>400 °C) slip system in quartz (Law, 1990).

When plotted in the sample reference frame, the misorientation axes outside of the shear zone in TJFA32c are clustered slightly asymmetrically around the X-axis and have a weak girdle through Y (Fig. 8b). The sheared sections of TJFA32c (Fig. 8a) do not contain the same girdle across Y as their unsheared counterpart (although this may relate to smaller sample sizes), but the strong clustering around X is common to both. A simple shear model using the shear zone kinematics

would predict a dominance in misorientation axes about Y, not the observed clustering of rotation axes about X.

Both inside and outside of the shear zone, the misorientation axis distributions of RW21a (Fig. 9c and d) in the sample reference frame display a large single cluster centred just off the Y-axis. Within the shear zone, this orientation of axes is not unexpected, as a rotation of subgrains about Y would be expected during simple shear. The observation that this dominance in rotation axes about Y occurs both inside and outside of the shear zone, however, suggests that the subgrain boundaries may not be uniquely attributed to the shear zone deformation.

There are three important observations that are illuminated by the misorientation axis distribution analyses: (1) where data is available for both sheared and unsheared sections of the same sample, the misorientation axis distributions are similar; (2) the misorientation axis distributions of samples RW21a and TJFA32c are different; and (3) the misorientation axes do not correspond in a simple way to the predictions of a simple kinematic model for the shear zones.

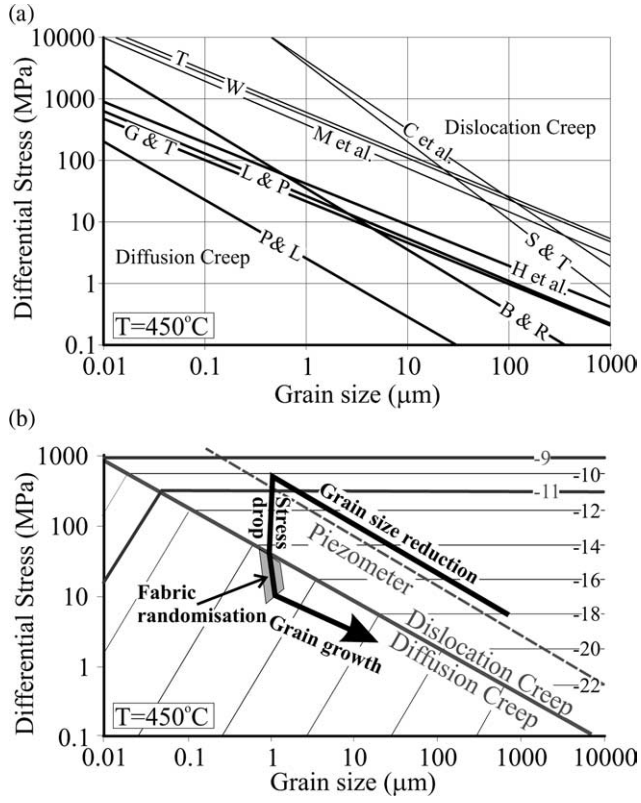

Fig. 9. Deformation mechanism maps for quartz. (a) Plot illustrating experimental constraints on the boundary between dislocation creep (upper right) and diffusion creep (lower left) in quartz at 450 °C (heavy lines) and the relationship between recrystallized grain-size and stress (palaeopiezometers shown by fine lines). Deformation mechanism boundaries are defined by the diffusion creep flow law of Brodie and Rutter (2000) and various dislocation creep flow laws (Paterson and Luan, 1990; Luan and Paterson, 1992; Gleason and Tullis, 1995; Brodie and Rutter, 2000; Hirth et al., 2001). Palaeopiezometers from Stipp and Tullis (2003), Christie et al. (1980), White (1979), Twiss (1977) and Mercier et al. (1977). (b) Boundary between dislocation and diffusion creep at 450 °C (bold grey line), calculated from power law creep and grain-size sensitive flow laws for quartz from Hirth et al. (2001) and Brodie and Rutter (2000), respectively, showing schematic stress path during shear zone deformation and fabric development (bold black line). Fine lines are contours of log strain-rate in s^{-1}; bold contours are preferred estimates of strain-rate from field data. Palaeopiezometer for recrystallized grain-size in quartz from Mercier et al. (1977) is also shown (dashed grey line).

7. Discussion

7.1. Deformation mechanisms and microstructural processes

The quartz veins analysed in this study have been demonstrably deformed in a coherent way to shear-strains of 5–15. Both inside and outside of the shear zone the samples have a relatively foam-like microstructure, with a large proportion of grains being internally strain free, although there is evidence for minor subgrain formation. The CPOs outside of the shear zone vary from a strong cross girdle, to very weak fabrics, yet inside of the shear zones, the quartz CPOs are uniformly weak to random. This implies that the deformation mechanisms active during shear zone deformation did not create a CPO and, at least in the case of RW21a, randomised a pre-existing CPO fabric during that shearing. Below, we will attempt to explain these microstructures in terms of the potential deformation mechanisms that formed them. It is important to note that none of these deformation mechanisms are mutually exclusive and that several may be active simultaneously during deformation.

7.1.1. Dislocation creep

At the estimated temperatures (450 ± 50 °C) and strain-rates (2×10^{-9}–2×10^{-11} s^{-1}) and with the grain-sizes observed in these rocks, one would predict that the dominant deformation mechanism accommodating the shearing in quartz would be dislocation creep or dislocation glide (Fig. 9). A shear-strain of 5–15 accommodated by dislocation creep should create a strong CPO that would overprint any existing CPO in the rocks (e.g. Lister, 1977; Tullis, 1977; Dell'Angelo and Tullis, 1989). However, only weak CPOs have been acquired, with RW21a illustrating a CPO fabric weakening into the shear zone of an older CPO that is distinctly preserved outside the shear zone.

Deformation by dislocation creep is usually accompanied by processes of recovery and recrystallization. Microstructural features such as subgrains and lobate grain boundaries are direct evidence of recovery and recrystallization processes. The veins show some subgrains and lobate boundaries, but these occur in both the sheared and unsheared sections. Contrary to initial expectations, there are slightly more low-angle boundaries in unsheared samples than sheared ones, misorientation axes are very similar inside and outside of the shear zones, and these axes do not mirror the macroscopic shear zone kinematics. The dislocation creep and associated processes that affected these veins affected all parts of the vein not just the strongly deformed segment inside the shear zones. If dislocation creep was the dominant process during initial shear zone deformation, then the microstructures and CPOs that must have been generated at that time have apparently been overprinted and destroyed by later processes.

7.1.2. Cataclasis

Discrete offsets and infilling veins are an indication that there was a brittle component to the shear deformation. We must consider whether shearing could also have been accommodated by brittle/frictional mechanisms. Cataclasis could explain the lack of CPO in the sheared veins. If cataclasis was the dominant deformation mechanism involved in the shearing, then one would expect the veins to be incoherent, displaced, or faulted at some scale and to show evidence for mixing and incorporation of the wall rocks into the shear zone. Most of the sheared veins, however, are smoothly and coherently deflected across the shear zones at both the macro- and micro-scales. Cataclasis also involves dilatancy. If the veins had been deformed cataclastically and later resealed by dissolution-precipitation creep or pressure solution processes, one would expect subtle differences under CL highlighting redeposition of quartz around angular fragments (Rusk and Reed, 2002; Muller et al., 2003). The ductilely sheared vein samples, however, are mostly featureless under CL. Dissolution-precipitation creep has been observed in some cases to result in a CPO with a strong X-maxima (e.g. Hippertt, 1994; Takeshita and Hara, 1998) that is not observed in data presented here. We conclude that the observations are inconsistent with the ductilely sheared veins having been deformed by a grain-scale cataclastic deformation mechanism.

7.1.3. Diffusion creep-accommodated grain boundary sliding (GBS)

Diffusion creep-accommodated GBS is often quoted as a deformation mechanism that takes place without the creation of a CPO (e.g. Kashyap and Mukherjee, 1985; Walker et al., 1990) and recent studies show that GBS associated with diffusion creep will weaken pre-existing CPOs (Jiang et al., 2000; Bestmann and Prior, 2003). Diffusion creep is grain-size sensitive. Diffusion creep at the microstructurally quenched grain-size of ~100 μm would require extremely low differential stress levels (~1 MPa), implying strain-rates of the order of $10^{-20}\,s^{-1}$ (Fig. 9a). At these strain-rates no significant shear-strain could be accumulated, especially over the 4 m.y. window available for these rapidly exhumed samples. Furthermore, experimental studies suggest that diffusion creep is very improbable at these grain-sizes, even in the presence of a fluid phase (Tullis and Yund, 1991; Brodie and Rutter, 2000). If diffusion creep was an important process, it probably would have required a much finer-grained shear zone microstructure. Direct evidence for diffusion creep is not always easy to find. Diffusion can lead to redistributions in major or trace elements. CL analyses show no significant features inside or outside the shear zones suggesting that there were no significant trace elements heterogeneities in the original quartz veins. We conclude that deformation by diffusion creep-accommodated GBS could explain the weak CPOs in the sheared veins. If this process occurred, however, it must have operated when the grain-size of the quartz veins was much finer than what we observe at the surface today.

7.1.4. Annealing and grain growth

The foam-like microstructure of both the sheared and unsheared samples implies that significant annealing and/or grain growth has occurred in the quartz veins after shear zone deformation. It has been shown (e.g. Shelley, 1989; Heilbronner and Tullis, 2002), that grain growth by itself does not destroy a CPO and in some circumstances it may even enhance CPO fabrics because of selective growth of preferred orientations (Neumann, 2000). Indeed, natural examples of annealed tectonites can have very strong CPOs (e.g. Trepmann and Stockhert, 2003). Stockhert and Duyster (1999) have suggested that 'discontinuous growth' could destroy a CPO due to the growth of grains that are crystallographically abnormally-oriented within a rock with a strong CPO. However, there is no evidence for this process in experimental studies of quartzite annealing (Heilbronner and Tullis, 2002). Moreover many decades of studies of annealing in metals shows that a 'discontinuous growth' mechanism will tend to develop strong CPOs (Humphreys and Hatherley, 1996). We conclude that although annealing and static grain growth must have occurred post-shearing, they cannot be invoked as CPO-destroying mechanisms.

7.2. A model for vein deformation

There is no simple way to explain the sheared vein microstructures. Deformation conditions suggest that dislocation creep should have occurred, yet there is no direct evidence of dislocation creep associated with these shear zones. Diffusion creep-accommodated grain boundary sliding could explain the weak CPOs, but this requires a much finer grain-size to have been present than that we observe today. We also have to explain the fact that sheared and unsheared vein microstructures are very similar. In this section we explore a composite model in which veins deform by dislocation creep, followed by diffusion creep prior to annealing and grain growth. In the model, veins undergo emplacement, shearing and grain-size reduction, stress-drop, further shearing and CPO destruction and, finally, annealing and grain growth, all in the presence of a high fluid pressure and under initially transiently high strain-rates.

A key to understanding these veins comes from the geodynamic context of their deformation. This predicts that individual veins were sheared during the up-ramping process in a short period of deformation, at transiently high stresses and strain-rate, but at a fixed temperature. Overburden pressure also remained relatively fixed during the deformation, reducing after deformation ceased as the Pacific Plate was exhumed by uplift and erosion. With these constraints in mind, variations in stress (or strain-rate) and grain-size can be used to understand the evolution of microstructures in these deformed veins. Fig. 9a shows experimental constraints on the boundary between diffusion and dislocation creep and on the relationship between recrystallized grain-size and stress (grain-size palaeopiezometers) for deformation in the dislocation creep field. To simplify the discussion, calculations we have made apply one deformation mechanism boundary and one palaeopiezometer.

We have chosen (arbitrarily) to use a deformation mechanism boundary defined by the diffusion creep flow law of Brodie and Rutter (2000), the dislocation creep flow law of Hirth et al. (2001) and the palaeopiezometer data of Mercier et al. (1977), as shown in Fig. 9b. Picking other data sets will change the numbers, but not the overall patterns or conclusions.

The chief uncertainty in the experimental rheological data, the deformation mechanism maps and the grain growth data is the role of fluids. The deformed quartz veins presented here were deformed in the presence of fluid, recorded in the form of syntectonic quartz-calcite veins that were emplaced into the shear zones during their ductile shearing in the shear zones. The deformation experienced by the sheared and deformed quartz veins took place under very wet conditions, recorded by the presence of fluid inclusions along grain boundaries.

7.2.1. Vein emplacement

Quartz veins emplaced into the Alpine Schist prior to the development of the Alpine foliation in the Mesozoic were dynamically recrystallized during Mesozoic Alpine deformation creating a strong CPO fabric (Vein A; Figs. 2b and 10a). These veins, and those emplaced after the Alpine foliation (Vein B; Figs. 2b and 10a), both have an annealed grain-shape microstructure due to static recrystallization during their prolonged late Cretaceous and younger residence in the lower crust of the Pacific Plate (Little, 2004). This static annealing did not alter the strong CPO in the veins deformed during the Mesozoic.

7.2.2. Shearing and grain-size reduction

Late Cenozoic deformation of the veins occurred when the rocks encountered the Alpine Fault ramp at depth, initiating shear zone formation (Fig. 10b). Shear zones were initiated as planar cracks in the brittlely deformed quartzofeldspathic host; however, they were blunted in the weaker, thick quartz veins into which the cracks terminated. Ductile shearing of the thick quartz veins (up to shear-strains of 5–10) was initially dominated by dislocation creep at transiently high stresses, creating a strong CPO in the deformed section of the veins (Fig. 10b). Dynamic recrystallization resulted in a marked reduction in grain-size (Fig. 10c). It is often suggested that a reduction in grain-size associated with recrystallization will cause a change in mechanism to diffusion creep (Rutter and Brodie, 1988; Vissers et al., 1995). In the case of quartz, a grain-size change by itself is insufficient because an accompanying drop in differential stress is also required (Brodie and Rutter, 2000). This is illustrated in Fig. 9a; quartz grain-size palaeopiezometers lie entirely in the dislocation creep field for a wide range of geologically reasonable creep stresses.

With strain-rate estimates of $2\times10^{-11}\,s^{-1}$–$2\times10^{-9}\,s^{-1}$ inferred for our deformed veins and a temperature of $450\pm50\,^{\circ}C$, the dislocation creep flow law of Hirth et al. (2001) suggests that mean differential stresses will have been between 369 and 1168 MPa (Fig. 9b). Although this latter stress estimate is slightly higher than most for stress states in the earth, differential stresses in the crust on the order of several hundreds of MPa have been documented (e.g. Brudy et al., 1997; Zoback and Townend, 2001). The quartz grain-size palaeopiezometer of Mercier et al. (1977) would estimate steady state grain-size of 1.04 and 0.2 μm, respectively, at these stresses. Prior et al. (1990) estimate rates of boundary migration associated with high stress-rates (5×10^{-9} MPa s^{-1}, ~150 MPa Ma^{-1}, which is probably much lower than the stress-rates experienced here) at 1.2×10^{-9} μm s^{-1}. These rates would suggest that a grain-size reduction of ~100 μm requires 2600 years of deformation. Although such calculations are approximations they indicate that grain-size reduction could easily keep pace with rapid deformation. Experimental data (Masuda et al., 1997) suggest considerably faster grain boundary migration rates.

7.2.3. Stress-drop

If grain-size during dislocation creep of quartzite is related to stress through any of the piezometer relationships shown in Fig. 9a, then the only practical way to move into the diffusion creep field is to reduce the differential stress (and strain-rate), whilst maintaining a fine grain-size. A stress-drop of several 100 MPa would be required (Fig. 9). This stress-drop must be fast relative to grain growth to allow diffusion creep to overprint the dislocation creep fabrics and enough strain must occur post-stress-drop for diffusion creep overprinting

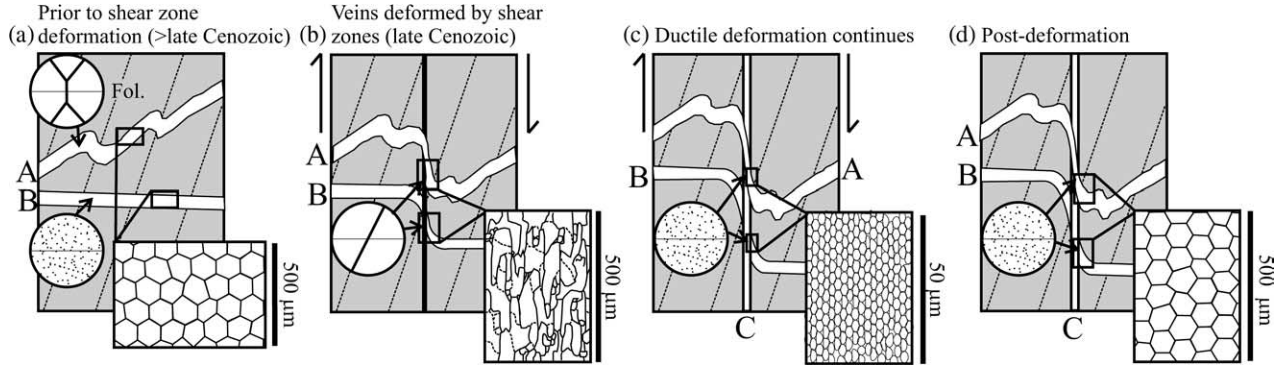

Fig. 10. Schematic diagram depicting different stages of vein deformation and the development of corresponding CPO fabrics. Enlargements of the microstructure are shown in boxes. CPOs are shown as skeleton fabrics on lower hemisphere equal area nets, with horizontal oriented parallel to the shear zone boundary except where specified. Veins A and B are emplaced pre- and post-Alpine foliation development, respectively.

of the previously imprinted CPO fabrics to occur. The cause of the stress-drop is interpreted to be passage of the upramped section past the high curvature toe of the Alpine Fault ramp and its associated high, localised differential stresses.

7.2.4. Shearing and CPO destruction

Shearing must continue after stress-drop to allow diffusion creep-accommodated GBS to destroy CPOs. The shear-strain required to significantly weaken CPOs is not constrained; we guess that shear-strains between 1 and 5 would be needed. In order for this to be accommodated in the time available—a maximum of about 4 Myr—then shear-strain-rates of 8×10^{-15} and $4\times10^{-14}\,s^{-1}$ are required for shear-strains of 1 and 5, respectively. The shear-strain-rates that can accumulate by diffusion creep depend upon the grain-size at the time of stress-drop. A grain-size of $\sim$1.04 μm would allow diffusion creep strain-rates of $\sim2.8\times10^{-15}\,s^{-1}$ at a differential stress of 40 MPa, whereas a grain-size of $\sim$0.2 μm would allow diffusion creep strain-rates of $\sim2\times10^{-13}\,s^{-1}$ at 121 MPa. These calculations suggest that, for the model to work, strain-rates and stresses must have been at the higher end of this estimate range. The high stress/strain-rate estimates would allow shear-strains of 1 and 5 to accumulate in the diffusion creep field in 0.14 and 0.69 Myr, respectively. The presence of fluid may enlarge the diffusion creep field on deformation mechanism maps (Tullis and Yund, 1991) and may allow quartz to deform by GBS at coarser grain-sizes and higher stresses than those predicted by the existing experiments. There cannot have been any significant grain growth whilst diffusion creep was operating because normal grain growth is very fast if the grain-size is very small, so that grains would grow rapidly to a size at which strain-rates controlled by diffusion creep would be very low. It is worth noting that experiments in the diffusion creep field in rocks (Walker et al., 1990; Tullis and Yund, 1991; Fliervoet et al., 1999; Brodie and Rutter, 2000), in ceramics (Chokshi, 2003) and in metals (Zelin et al., 2002) are conducted with little change in grain-size during the deformation. Although in some cases grain growth is deliberately suppressed by additives to pin grain boundaries (Walker et al., 1990), the experiments suggest that constant grain-size is maintained during diffusion creep.

7.2.5. Annealing and grain growth

Both the sheared and unsheared sections of the veins display annealed, nearly foam-like microstructures, with an average grain-size of 80–100 μm. If the sheared parts of the veins have been reduced to a very fine grain-size of 1 μm or less, they have later grown to their present grain-size (Fig. 10d). There are two questions that need addressing: (1) is the grain growth from 1 to 100 μm realistic in 4 m.y., and (2) to what grain-size would the unsheared matrix grow in the same time period? Static grain growth occurs at an inverse exponential rate, with growth-rates dropping off with increasing grain-size (Humphreys and Hatherley, 1996):

$$D^{1/n} - D_0^{1/n} = kt \tag{1}$$

$$k = K_0 e^{(-Q/RT)} \tag{2}$$

where D is the grain diameter at time t and D_0 is the grain diameter at time $t=0$, K_0 and n are constants, Q is the activation energy, R is the gas constant and T the absolute temperature. If the shear zone and wall-rock have different initial grain-sizes (D_{ISZ} and D_{IWR}), then the final grain-sizes of the wall-rock (D_{FWR}) and shear zone (D_{FSZ}) are a function of n:

$$D_{FWR}^{1/n} = D_{FSZ}^{1/n} + D_{IWR}^{1/n} - D_{ISZ}^{1/n} \tag{3}$$

Fig. 11 shows the results of some numerical experiments in which the grain-size in the shear zone grows from 1 μm at the same time as the wall-rock grows from 80 μm. These show that as long as $1/n \geq 3$ then the final grain-size in both shear zone and wall-rock will be very similar. Experimental quartz grain growth $1/n$ values are best constrained at 3 or greater (Tullis and Yund, 1982; Masuda et al., 1997) so it is likely that a fine-grained shear zone microstructure could grow to a grain-size indistinguishable from its wall rock.

Calculating the time required for growth from 1 to $\sim$100 μm is not straightforward as quartz growth rate is a function of temperature, pressure and water content (Tullis and Yund, 1982). It is not clear whether we should apply fluid pressure or lithostatic pressure estimates to grain-growth calculations. Tullis and Yund (1982) estimate that fluid pressure was close to total pressure in their experiments. An empirical growth-rate equation derived from data of Tullis and Yund (1982), which is also pressure (P) sensitive, is:

$$D^{3.2} - D_0^{3.2} = 4.96P^{2.34}e^{(-215/RT)}t \tag{4}$$

where $K_0 = 4.96P^{2.34}$, $1/n = 3.2$ and $Q = 215$ kJ mol^{-1}. Times for growth from 1 to 100 μm at 450 °C and 310 MPa (post-failure fluid pressure) are estimated at 85 Ma, which is longer than the time available. It is likely that fluid pressures post-shear failure increased again to close to lithostatic pressures, $\sim$550 MPa (Wightman et al., submitted); this pressure, with temperatures at the upper limit of the estimates (500 °C),

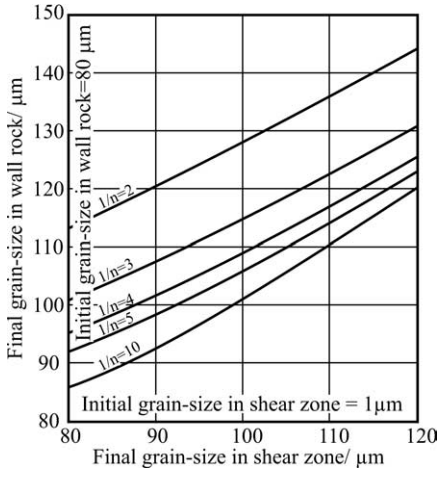

Fig. 11. Plot of results of numerical grain growth experiments showing variation in final grain-size of quartz in the shear zone against the final grain-size in the wall rock using different grain growth exponents. Initial grain-size in the shear zones is 1 μm; initial grain size in veins in the wall rock is 80 μm.

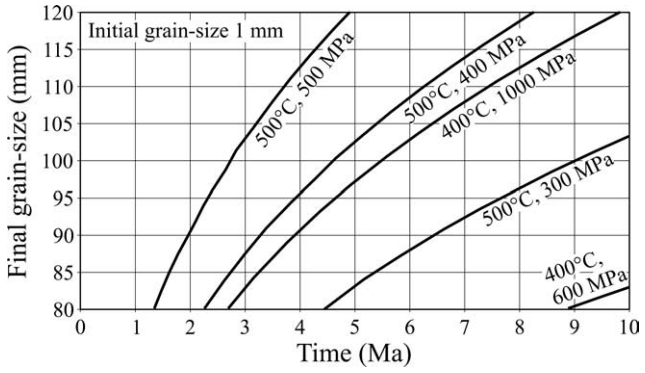

Fig. 12. Graph showing grain growth over time as a function of ambient temperatures and fluid pressures and an initial grain-size of 1 μm. An empirical growth-rate equation derived from data of Tullis and Yund (1982) was used.

allows growth in the available time to become possible, ~2–3 Myrs (Fig. 12). Varying the initial grain-size (up to ~10 μm) has no significant effect. Given the uncertainties in the extrapolation of experimental data to geological conditions we conclude that growth of a fine-grained shear zone microstructure to ~100 μm in a few million years cannot be ruled out, especially as it is likely that the veins were very wet and grain growth-rates may have been faster than experimental predictions since the dominant control on grain growth in wet quartz is its solubility into a grain boundary fluid (Tullis and Yund, 1982, 1989; Farver and Yund, 2000).

7.3. Deformation during transiently high stress

Changing deformation conditions, including transiently high stresses, can lead to non-steady state deformation, resulting in changes in the dominant deformation mechanisms that are active. These changes in deformation mechanism may create a wide range of microstructures in rocks that have only slightly different stress and strain-rate deformation histories. A deformation path similar to our model presented here, also involving transiently high stresses, was proposed by Trepmann and Stockhert (2003) invoking dislocation glide and creep as the dominant deformation mechanisms at relatively low temperatures, resulting in the formation and preservation of a strong CPO fabric.

These two models are not mutually exclusive; a random CPO is not the only microstructure our shear zone deformation model (Fig. 9b) could produce. Small changes in the stress conditions during deformation would result in the formation of very different microstructures; these include: (1) initial differential stress conditions that are not as high as required by our model. This would result in a coarser recrystallized grain-size and the subsequent stress drop would not be sufficient to allow diffusion creep-accommodated GBS to become the dominant deformation mechanism; (2) initial differential stresses that are very high but the stress drop after initial dislocation creep-accommodated deformation is not sufficient to drop deformation into the diffusion creep regime; and (3) an increase in stress after diffusion creep dominated deformation that allows deformation to re-enter the dislocation creep regime and intracrystalline strain accumulates. Any of these possibilities would result in the formation of a strong CPO, much like that recorded by Trepmann and Stockhert (2003), highlighting the importance of different active deformation mechanisms in the formation of microstructures under transient stress conditions.

8. Conclusions

Observations made on natural rocks deformed in shear zones in the Southern Alps, New Zealand, provide a model for the processes that may occur during short-lived deformation at transiently high stresses at mid-crustal levels:

1. Veins that have been ductilely sheared to shear-strains of 5–15 have weak to random CPO, but microstructures that are identical to the unsheared section of the vein outside of the shear zone.
2. The microstructure and fabrics recorded in these shear zones cannot be explained by a simple one-deformation mechanism model. In order to achieve the observed microstructure, we need to invoke a deformation model that involves both dislocation and diffusion creep during the shearing event, with the latter acting to weaken and destroy the initially strong dislocation creep created CPO.
3. Transient differential stress and strain-rate conditions are necessary to allow deformation to switch from dislocation creep to the diffusion creep regime through a combination of grain-size reduction and a significant stress-drop post-failure.
4. The tectonic framework of these shear zones give validity to the deformation model. Transiently high stresses and strain-rates created due to backtilting of the Pacific Plate onto the Alpine Fault ramp cause backshears to initiate at 18–23 km depth, with deformation initially accommodated by dislocation creep processes with rapid grain size reduction. Stresses around the shear zones drop significantly once the rocks have been tilted onto the fault ramp, allowing diffusion creep and GBS to become dominant. As the rocks are passively translated up the fault ramp, stresses relax completely and grain growth and annealing occurs. Time constraints on grain growth from experimental data suggest that grain growth from an initial grain size of 1 μm to the observed microstructure would require 2–3 Ma. This rate may be greatly enhanced by the presence of fluid, but still falls within the 3–4 Myrs required to translate and exhume the shear zones up the Alpine Fault from 18 to 23 km depth.

Acknowledgements

The authors would like to thank John Wheeler, Richard Holme, Michel Bestmann, Sandra Piazolo and Julian Mecklenburgh for helpful discussion during preparation of the manuscript, Jan Tullis for helping re-analyse the grain-growth data, G. Lloyd and T. Takeshita for reviewing the manuscript

and Kees Veltcamp for help with the CL analyses. The authors wish to acknowledge funding from Bright Futures Top Achievers Doctoral Scholarship to Wightman.

References

Barnhoorn, A., Bystricky, M., Burlini, L., Kunze, K., 2004. The role of recrystallisation on the deformation behaviour of calcite rocks: large strain torsion experiments on Carrara Marble. Journal of Structural Geology 26 (5), 885–903.

Behrmann, J.H., Mainprice, D., 1987. Deformation mechanisms in a high temperature quartz-feldspar mylonite: evidence for superplastic flow in the lower continental crust. Tectonics 140, 297–305.

Bestmann, M., Prior, D.J., 2003. Intragranular dynamic recrystallisation in naturally deformed calcite marble: diffusion accommodated grain boundary sliding as a result of subgrain rotation recrystallisation. Journal of Structural Geology 25 (10), 1597–1613.

Bestmann, M., Prior, D.J., Veltkamp, K., 2004. Fluid assisted diffusional creep as a possible shape-controlling process for σ-shaped porphyroblasts within a calcite marble shear zone. Journal of Structural Geology 26, 869–883.

Borghi, A., Spiess, R., 2004. Studying metamorphic microstructures: a brief insight on modern methodological approaches. Periodico di Mineralogia 73 (2), 235–247.

Braun, J., Beaumont, C., 1995. Three-dimensional numerical experiments of strain partitioning at oblique plate boundaries: Implications for contrasting tectonic styles in the southern Coast Ranges, California, and central South Island, New Zealand. Journal of Geophysical Research 100 (B9), 18059–18074.

Brodie, K.H., Rutter, E.H., 2000. Deformation mechanisms and rheology: why marble is weaker than quartzite. Journal of Geological Society of London 157, 1093–1096.

Brudy, M., Zoback, M.D., Fuchs, K., Rummel, F., Baumgartner, J., 1997. Estimation of the complete stress tensor to 8 km depth in the KTB scientific drill holes: implications for crustal strength. Journal of Geophysical Research 102 (B8), 18453–18475.

Brunel, M., 1980. Quartz fabrics in shear-zone mylonites: evidence for a major imprint due to late strain increments. Tectonophysics 64, 33–44.

Bull, W.B., Cooper, A.F., 1986. Uplifted marine terraces along the Alpine Fault, New Zealand. Science 234, 1225–1228.

Chokshi, A.H., 2003. Diffusion, diffusion creep and grain growth characteristics of nanocrystalline and fine-grained monoclinic, tetragonal and cubic zirconia. Scripta Materialia 48 (6), 791–796.

Christie, J.M., Ord, A., Koch, P.S., 1980. Relationship between recrystallised grainsize and flow-stress in experimentally deformed quartzite. Transactions of American Geophysical Union 61, 377.

De Mets, C., Gordon, R.G., Argus, D.F., Stein, S., 1994. Effect of recent revisions to the geomagnetic reversal time scale on estimates of current plate motions. Geophysical Research Letters 21, 2191–2194.

Dell'Angelo, L., Tullis, J., 1989. Fabric development in experimentally sheared quartzites. Tectonophysics 169, 1–22.

Farver, J.R., Yund, R.A., 2000. Silicon diffusion in a natural quartz aggregate: constraints on solution-transfer diffusion creep. Tectonophysics 325, 193–205.

Fliervoet, T.F., White, S.H., 1995. Quartz deformation in a very fine grained quartzofeldspathic mylonite: a lack of evidence for dominant grain boundary sliding deformation. Journal of Structural Geology 17 (8), 1095–1109.

Fliervoet, T.F., Drury, M.R., Chopra, P.N., 1999. Crystallographic preferred orientations and misorientations in some olivine rocks deformed by diffusion or dislocation creep. Tectonophysics 303, 1–27.

Gleason, G.C., Tullis, J., 1995. A flow law for dislocation creep of quartz aggregates determined with the molten salt cell. Tectonophysics 247, 1–23.

Gleason, G.C., Tullis, J., Heidelbach, F., 1993. The role of dynamic recrystallization in the development of lattice preferred orientations in experimentally deformed quartz aggregates. Journal of Structural Geology 15 (9/10), 1145–1168.

Grapes, R.H., 1995. Uplift and exhumation of Alpine Schist, Southern Alps, New Zealand: thermobarometric constraints. New Zealand Journal of Geology and Geophysics 38, 525–533.

Heilbronner, R., Tullis, J., 2002. The effect of static annealing on microstructures and crystallographic preferred orientations of quartzites experimentally deformed in axial compression and shear. In: De Meer, S., Drury, M.R., De Bresser, J.H.P., Pencock, G.M. (Eds.), Deformation Mechanisms, Rheology and Tectonics: Current Status and Future Perspectives. Geological Society, London, Special Publications 200, pp. 191–218.

Hill, M., 2005. Crystallographic preferred orientation of quartz and calcite in brittle-ductile shear arrays from the Southern Alps of New Zealand. Unpublished Master of Science thesis, Victoria University of Wellington.

Hippertt, J.F., 1994. Microstructures and c-axis fabrics indicative of quartz dissolution in sheared quartzites and phyllonites. Tectonophysics 229 (3-4), 141–163.

Hirth, G., Tullis, J., 1992. Dislocation creep regimes in quartz aggregates. Journal of Structural Geology 14 (2), 145–159.

Hirth, G., Teyssier, C., Dunlap, W.J., 2001. An evaluation of quartzite flow laws based on comparisons between experimentally and naturally deformed rocks. International Journal of Earth Sciences 90, 77–87.

Humphreys, F.J., Hatherley, M., 1996. Recrystallisation and related annealing phenomena. Pergamon Press, New York.

Jiang, Z., Prior, D.J., Wheeler, J., 2000. Albite crystallographic preferred orientation and grain misorientation distribution in a low-grade mylonite: implications for granular flow. Journal of Structural Geology 22, 1663–1674.

Kashyap, B.P., Mukherjee, A.K., 1985. On the models for superplastic deformation. In: Baudelet, B., Suery, M. (Eds.), Superplasticity. CNRS, Paris, pp. 4.1–4.31.

Koons, P.O., 1989. The topographic evolution of collisional mountain belts: a numerical look at the Southern Alps, New Zealand. American Journal of Science 289, 1041–1069.

Kretz, R., 1983. Symbols for rock-forming minerals. American Mineralogist 68, 277–279.

Law, R.D., 1990. Crystallographic fabrics: a selective review of their applications to research in structural geology. In: Knipe, R.J., Rutter, E.H. (Eds.), Deformation Mechanisms, Rheology and Tectonics. Geological Society, London, Special Publications 54, pp. 335–352.

Lister, G.S., 1977. Crossed-girdle c-axis fabrics in quartzites plastically deformed by plane strain and progressive simple shear. Tectonophysics 39, 51–54.

Little, T.A., 2004. Transpressive ductile flow and oblique ramping of lower crust in a two-sided orogen: insight from quartz grain-shape fabrics near the Alpine Fault, New Zealand. Tectonics 23, TC2013. doi:10.1029/2002TC0011456.

Little, T.A., Holcombe, R.J., Ilg, B.R., 2002. Ductile fabrics in the zone of active oblique convergence near the Alpine Fault, New Zealand; identifying the neotectonic overprint. Journal of Structural Geology 24 (1), 193–217.

Little, T.A., Cox, S.C., Vry, J., Batt, G.E., 2005. Variations in exhumation level and uplift-rate related to oblique-slip ramp geometry, Alpine Fault, central Southern Alps, New Zealand. GSA Bulletin 117, 724–735.

Lloyd, G.E., 1987. Atomic number and crystallographic contrast images with the SEM: a review of backscattered techniques. Mineralogical Magazine 51, 3–19.

Lloyd, G.E., Farmer, A.B., Mainprice, D., 1997. Misorientation analysis and the formation and orientation of subgrain and grain boundaries. Tectonophysics 279, 55–78.

Luan, F.C., Paterson, M.S., 1992. Preparation and deformation of synthetic aggregates of quartz. Journal of Geophysical Research 97 (B1), 301–320.

Masuda, T., Morikawa, T., Nakayama, Y., Susuki, S., 1997. Grain-boundary migration of quartz during annealing experiments at high temperatures and pressures, with implications for metamorphic geology. Journal of Metamorphic Geology 15, 311–322.

Mercier, J.C.C., Anderson, D.A., Carter, N.L., 1977. Stress in the lithosphere. Inferences from steady state flow of rocks. Pure and Applied Geophysics 115, 199–226.

Muller, A., Wiedenbeck, M., Van der Kerkhof, A.M., Kronz, A., Simon, K., 2003. Trace elements in quartz—a combined electron microprobe, secondary ion mass spectrometry, laser-ablation ICP-MS, and cathodoluminescence study. European Journal of Mineralogy 15 (4), 747–763.

Neumann, B., 2000. Texture development of recrystallised quartz polycrystals unravelled by orientation and misorientation characteristics. Journal of Structural Geology 22, 1695–1711.

Norris, R.J., Koons, P.O., Cooper, A.F., 1990. The obliquely-convergent plate boundary in the South Island of New Zealand: implications for ancient collision zones. Journal of Structural Geology 12 (5/6), 715–725.

Orzol, J., Trepmann, C.A., Stockhert, B., Shi, G., 2003. Critical shear stress for mechanical twinning of jadeite: an experimental study. Tectonophysics 372 (3–4), 135–145.

Paterson, M.S., Luan, F.C., 1990. Quartzite rheology under geological conditions. In: Knipe, R.J., Rutter, E.H. (Eds.), Deformation Mechanisms, Rheology and Tectonics. Geological Society, London, Special Publications 54, pp. 299–307.

Pieri, M., Burlini, L., Kunze, K., Stretton, I., Olgaard, D.L., 2001. Rheological and microstructural evolution of Carrara marble with high shear strain: results from high temperature torsion experiments. Journal of Structural Geology 23 (9), 1393–1413.

Prior, D.J., Knipe, R.J., Handy, M.R., 1990. Estimates of the rates of microstructural changes in mylonites. In: Knipe, R.J., Rutter, E.H. (Eds.), Deformation Mechanisms, Rheology and Tectonics. Geological Society, London, Special Publications 54, pp. 309–319.

Prior, D.J., Boyle, A.P., Brenker, F., Cheadle, M.C., Day, A., Lopex, G., Peruzzo, L., Potts, G.J., Reddy, S., Spiess, R., Timms, N.E., Trimby, P.W., Wheeler, J., Zetterstrom, L., 1999. The application of electron backscatter diffraction and orientation contrast imaging in the SEM to textural problems in rocks. American Mineralogist 84, 1741–1759.

Prior, D.J., Wheeler, J., Peruzzo, L., Spiess, R., Storey, C., 2002. Some garnet microstructures: an illustration of the potential of orientation maps and misorientation analysis in microstructural studies. Journal of Structural Geology 24, 999–1011.

Rusk, B., Reed, M., 2002. Scanning electron microscope-cathodoluminscence analysis of quartz reveals complex growth histories in veins from the Butte porphyry copper deposit, Montana. Geology 30 (8), 727–730.

Rutter, E.H., Brodie, K.H., 1988. The role of tectonic grain size reduction in the rheological stratification of the lithosphere. Geologische Rundschau 77, 295–308.

Schmid, S.M., 1982. Microfabric studies as indicators of deformation mechanisms and flow laws operative in mountain building. In: Hsu, K.J. (Ed.), Mountain Building Processes. Academic Press, London, pp. 95–110.

Schmid, S.M., Casey, M., Starkey, J., 1981. An illustration of the advantages of a complete texture analysis described by the orientation distribution function (ODF) using quartz pole figure data. Tectonophysics 78, 101–117.

Shelley, D., 1989. Plagioclase and quartz preferred orientations in a low-grade schist: the roles of primary growth and plastic deformation. Journal of Structural Geology 11 (8), 1029–1038.

Stipp, M., Tullis, J., 2003. The recrystallised grain size piezometer for quartz. Geophysical Research Letters 30 (21), 2088.

Stockhert, B., Duyster, J., 1999. Discontinuous grain growth in recrystallised vein quartz—implications for grain boundary structure, grain boundary mobility, crystallographic preferred orientation, and stress history. Journal of Structural Geology 21, 1477–1490.

Takeshita, T., Hara, I., 1998. C-axis fabrics and microstructures in a recrystallized quartz vein deformed under fluid-rich greenschist conditions. Journal of Structural Geology 20 (4), 417–431.

Trepmann, C.A., Stockhert, B., 2003. Quartz microstructures developed during non-steady state plastic flow at rapidly decaying stress and strain rate. Journal of Structural Geology 25, 2035–2051.

Trimby, P.W., Prior, D.J., Wheeler, J., 1998. Grain boundary hierarchy development in a quartz mylonite. Journal of Structural Geology 20 (7), 917–935.

Tullis, J., 1977. Preferred orientation of quartz produced by slip during plane strain. Tectonophysics 39, 87–102.

Tullis, J., Yund, R.A., 1982. Grain growth kinetics of quartz and calcite aggregates. Journal of Geology 90, 301–318.

Tullis, J., Yund, R.A., 1989. Hydrolytic weakening of quartz aggregates: the effects of water and pressure on recovery. Geophysical Research Letters 16 (11), 1343–1346.

Tullis, J., Yund, R.A., 1991. Diffusion creep in feldspar aggregates: experimental evidence. Journal of Structural Geology 13 (9), 987–1000.

Twiss, R.J., 1977. Theory and applicability of a recrystallised grain size palaeopiezometer. Pure and Applied Geophysics 115, 227–244.

Vissers, R.L.M., Drury, M.R., Hoogerduijn Straating, E.H., Spiers, C.J., Van der Wal, D., 1995. Mantle shear zones and their effect on lithosphere strength during continental breakup. Tectonophysics 249, 155–171.

Vry, J., Baker, J., Maas, R., Little, T.A., Grapes, R.H., Dixon, M., 2004. Zoned (Cretaceous and Cenozoic) garnet and the timing of high grade metamorphism, Southern Alps, New Zealand. Journal of Metamorphic Geology 22 (3), 137–157.

Walcott, R.I., 1998. Modes of oblique compression: late Cenozoic tectonics of the South Island of New Zealand. Reviews of Geophysics 36 (1), 1–26.

Walker, A.N., Rutter, E.H., Brodie, K.H., 1990. Experimental study of grain-size sensitive flow of synthetic, hot-pressed calcite rocks. In: Knipe, R.J., Rutter, E.H. (Eds.), Deformation Mechanisms, Rheology and Tectonics. Geological Society, London, Special Publications 54, pp. 259–284.

Wellman, H.W., 1979. An uplift map for the South Island of New Zealand and a model for the uplift of the Southern Alps. Royal Society of New Zealand Bulletin, 18.

Wenk, H.-R., 1985. Carbonates. In: Wenk, H.-R. (Ed.), Preferred Orientations in Deformed Metals and Rocks: an Introduction to Modern Texture Analysis. Academic Press, Orlando, pp. 361–384.

Wenk, H.-R., Christie, J.M., 1991. Comments on the interpretation of deformation textures in rocks. Journal of Structural Geology 13, 1091–1110.

Wheeler, J., Trimby, P.W., Prior, D.J., Jiang, Z., Spiess, R., 2001. The petrological significance of misorientations between grains. Contributions to Mineralogy and Petrology 141 (1), 109–124.

White, S.H., 1979. Grainsize variation across a mylonite zone. Contributions to Mineralogy and Petrology 70, 193–203.

Wightman, R.H., Little, T.A., Baldwin, S.L., Valley, J., submitted. Stress, fluid pressure cycling and transient deep embrittlement of the lower crust recorded in a paleo-brittle-ductile transition zone beneath the Southern Alps, New Zealand. Journal of Geophysical Research.

Zelin, M., Gershon, B., Arbel, I., 2002. Grain growth during superplastic deformation. Interface Science 10 (1), 37–42.

Zoback, M.D., Townend, J., 2001. Implications of hydrostatic pore pressures and high crustal strength for the deformation of intraplate lithosphere. Tectonophysics 336 (1–4), 19–30.